 doi:10.20944/preprints202106.0191.v1

Article

Effect of Grit Blasting and Polishing Pretreatments on the Microhardness, Adhesion and Corrosion Properties of Electrodeposited Ni-W/SiC Nano-composite Coatings on 45 Steel Substrate.

Gbenontin V Bertrand[1], Min Kang[1,*], Ndumia Joseph Ndiithi[1], Samuel Mbugua Nyambura[1], Awuah Emmual[1] and Yin Zhang [1].

[1] College of Engineering, Nanjing Agricultural University, Nanjing 210031, China; 2019212016@njau.edu.cn (G.V.B.); accessmbugua@gmail.com (S.M.N.); eawuah12@gmail.com (A.E); 2020212023@stu.njau.edu.cn (N.J.N.); 2018212003@njau.edu.cn (Y.Z.).

* Correspondence: kangmin@njau.edu.cn; Tel.: +86-25-5860-6667

Abstract : In this study, grit blasting pretreatment was used to improve the adhesion and corrion resistance and microhardness of Ni-W/SiC nanocomposite coatings fabricated using conventional electrodeposition technique. Prior to deposition, grit blasting and polishing (more commonly used) pretreatment were used to prepare the surface of the substrate and the 3D morphology of the pretreated substrates was characterized using laser scanning confocal microscopy. The coatings surface and the cross section morphology were analyzed using scanning electron microscopy (SEM). The chemical composition, crystalline structure, microhardness, adhesion, and the corrosion behavior of the deposited coatings were characterized using energy dispersive spectroscopy (EDS), X-ray diffraction (XRD), microhardness tester, scratch tester and electrochemical workstation, respectively. The results indicated that the grit blasting and SiC addition, improved the microhardness, adhesion and corrosion resistance. The Ni-W-SiC nanocomposites pretreated by grit blasting exhibited the best adhesion strength, up to 36.5 ± 0.75 N. Its hardness was the highest and increased up to 673 ± 5.47Hv and its corrosion resistance was the highest compared to the one pretreated by polishing.

Keywords: nano-composite; blasting; pretreatment; adhesion; microhardness, corrosion resistance

1. Introduction

World's food need is increasing and we must ensure the food security of the present and future generation. This increase in food requirements is due to the increase in the population of each country in turn worldwide. On the one hand, we have witnessed the migration of labor from some countries to cities where non-agricultural occupations lead to the reduction of agricultural labor and, subsequently, the high cost of labor. This makes the production of some agricultural goods uncompetitive. In addition, manual agriculture does not allow rapid production and harvesting, nor does it allow the planting of several hectares of arable land in order to satisfy food needs and also to be competitive. Agricultural mechanization is one of the major solutions to this problem. Agricultural mechanization can help the sustainable development of world food systems by increasing output production and reducing lost foods through the production chain. Several

Preprints (www.preprints.org) | NOT PEER-REVIEWED | Posted: 7 June 2021 doi:10.20944/preprints202106.0191.v1

countries have established an agricultural development policy, which is reflected in the use of agricultural machinery from soil preparation, through planting, to harvesting and processing. Among these machines we can mention tillage equipment, Sseed Ssowing Eequipment, planting machinery, harvesting machinery, irrigation and drainage machinery [1]. It is known that wear and corrosion are major reasons for the failure of mechanical parts [2] . During its use, the agricultural machinery deals with different kinds of environmental conditions, soil, plants, pesticide, fertilizers, and post-harvest processing due to reaction between agriculture machines and these conditions expose the parts to wear such as adhesive, abrasive, fatigue, erosion, chemical, and corrosion [3]. This is the case with the harvester blade (wear, stem damage, corrosion etc.), the main part that is in direct contact with the soil and agricultural product. Solving the corrosion and wear problem leads to an increase in blade life, improved blade cutting quality, reduced replacement time for worn blades, and reduced labor costs [4,5]. Many surface treatment techniques such as : Hhot Ddipping, surface hardening, thermal spraying, metallic cementation, nitrocarburizing, plasma nitriding, hard facing, and electrodeposition [6–8] can be used to improve the microhardness, corrosion and wear resistance of mechanical tools. Nanocomposite coating is a new trend to promote surface properties of the different metals used in manufacturing agricultural machinery. Electrodoposition technology has been used extensively in recent years for the preparation of protective coatings because it is less expensive and more convenient for engineering applications. This method has been used in the development of protective coatings basing on the metals or the alloys. Among these coatings, Ni-W alloy coating has caught the attention of several researchers and has been proposed because of its corrosion resistance, its hardness and its low toxicity to replace hard chromium. In general, research carried out on electrodeposited Ni-W alloy coatings is concerned with improving their wear resistance, hardness, and corrosion resistance [9– 12]. In addition to the metal or alloy matrix, nano particles are widely added to have a coating which can always exhibit the better mechanical and corrosion properties [13–18]. For this reason, many researchers have worked on Ni-W nanocomposite coatings and some studies have shown the performance of the incorporation of different nanoparticles in this binary alloy. Furthermore, A number of investigations have been performed on the electrodeposition of the Ni–W–SiC composite system and many of them have been done using the polishing pretreatment for the sample [19–21]. Moreover, Currently there are few or no studies available on the effects of the different pretreatment methods on Ni-W-SiC nanocomposite. Or it has known in many cases involving mechanical loading, failure occurs at the interface between the coating and the substrate. Through literature, the surface roughness of the substrate surface is increased at the macro-level by blasting technique and this removes the inherent oxide layers that are present on the substrate surface, and improves the interaction between the coating and substrate thereby enhancing adhesion,corrosion and wear resistance properties [22-24]. Grit blasting has also been reported to impart near-surface compressive residual stress which decreases effective applied stress during service as well as delaying formation and propagation of microcracks on the bulk material surface where the coating has a good adherence to the substrate surface and is free of defects and

Preprints (www.preprints.org) | NOT PEER-REVIEWED | Posted: 7 June 2021 doi:10.20944/preprints202106.0191.v1

discontinuities [22]. It has been reported that the Ni-B coatings deposited on the 8620H steel substrates carried out with sandblasting by emery powders had the best adhesion strength and corrosion resistance[24].

In this study, Ni-W-SiC nanocomposites coatings are prepared by conventional electrodeposition. The effects of two different pretreatment processes (grit blasting and polishing pretreatment) on the coating adhesion, microhardness and corrosion resistance of Ni-W-SiC nanocomposite coatings have been studied. In this study we expect that the pretreatment using grit blasting could confer a rougher morphology, an improvement of the adhesion, the microhardness and corrosion resistance of the coating.

2. Materials and Methods

Ni-W/SiC nanocomposite coatings were deposited on 45 steel samples measuring 30 mm × 8 mm × 7 mm using conventional electrodeposition technique. For the first phase, steel samples were pretreated using steel grit blasting technique and then rinsed thoroughly in an electrostatic agitator using double distilled water to remove any loose metal pieces. The grit blasted samples (Figure 1a) were subjected to a triple-immersion pretreatment process for electric cleaning. They were then immersed into the electrolyte for the deposition process. Grit blasting was performed by abrasive grit blasting machine with a 18 mesh steel grit particles at a pressure of 0.6 MPa. The schematic of grit blasting machine is shown in Figure 2.

For comparison purposes, Ni-W/SiC nanocomposite coatings were also deposited on 45 steel substrates pretreated using polishing pretreatment process (Figure 1b). For this phase of the experiment, the substrates were mechanically polished using abrasive emery papers with different granulometry ranging from 320-2000 and then subjected to a triple-immersion pretreatment process for electric cleaning. This ensured a stronger bond between the coating and substrate surface. The pretreatment process comprised of degreasing using electro-hydrostatic fluid, removal of oxide layer on the surface by passing using a strong activating solution, and lastly removal of carbon-black using a weak activating solution. Table 1 shows the degreasing solution and HCl pickling solution reagents that were used for the process. The electrodeposition process was carried out in a 1000 ml glass beaker, and the electrodes were immersed vertically into the aqueous electrolytic Watts solution with a distance of 3 cm between them.

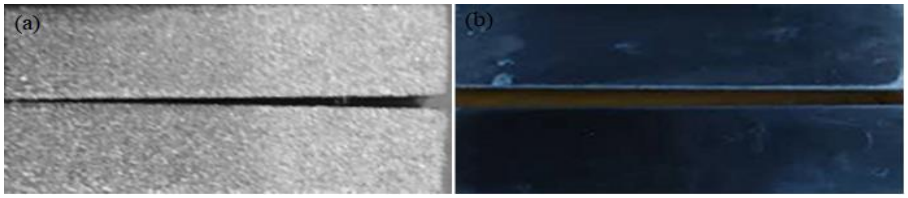

Figure 1. (**a**) Grit blasted sample, (**b**) Polished samples.

Preprints (www.preprints.org) | NOT PEER-REVIEWED | Posted: 7 June 2021 doi:10.20944/preprints202106.0191.v1

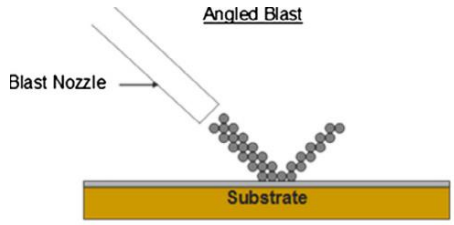

Figure 2. Schematic of grit blast operation[22]

Table 1. Pre-treatment process of substrate surface.

Process	Fluid Type	Chemical Composition	Concentration ($g \cdot L^{-1}$)
Degreasing	Electro-hydrostatic fluid	NaOH	25
		Na_2CO_3	21.7
		Na_3PO_4	50
		NaCl	2.4
Pickling	Strong Activation Solution	HCl	25
		NaCl	140.1
	Weak Activation Solution	$NaC_6H_5O_7 \cdot 2H_2O$	141.2
		$H_3C_6H_5O_7 \cdot H_2O$	94.2
		$NiCl_2 \cdot H_2O$	3

SiC nanoparticles with an average particle size of 40 nm were dispersed in the aqueous sulphate-citrate electrolyte. Prior to the deposition process, the solutions with SiC nanoparticles were stirred by continuous magnetic stirrer at a rate of 360 rpm for at least 24 h and subsequently by ultrasonic agitation for 30 min just prior to electrodeposition to ensure uniform dispersion of SiC and prevent its agglomeration and settling. The same rate of magnetic stirring was also employed during electrodeposition at the cell bottom in order to maintain a homogeneous concentration of SiC particles in the solution. The reagents with without any other form of purification were used in the electrolyte. Double distilled water was used to prepare the electrolyte. The chemical composition of the electrolyte and the function of each component are shown in Table 2.

Table 2. Chemical composition of the electrolyte bath.

Bath component	Concentration ($g \cdot L^{-1}$)	Function
Nickel sulphate ($NiSO_4 \cdot 7H_2O$)	18	Ni source
Sodium tungstate ($Na_2WO_4 \cdot 2H_2O$)	46	W source
Trisodium citrate dihydrate ($Na_3C_6H_5O_7 \cdot 2H_2O$)	145	Complexer for Ni and W
Sodium bromide (NaBr)	16	Conductivity increase
Sodium dodecyl sulphate (SDS)	0.3	Surfactant
Ammonium Chloride (NH_4Cl)	26	Buffer
SiC (40 nm)	0, 3, 6,12	Nanoparticles

Preprints (www.preprints.org) | NOT PEER-REVIEWED | Posted: 7 June 2021 doi:10.20944/preprints202106.0191.v1

The electrolyte bath temperature was raised to 60 ℃ to facilitate the effective transfer of electrons and a current density of 5 A.dm^{-2} was used throughout the experiment. Table 3 shows the operating parameters used for preparing the Ni-W binary and Ni-W/SiC nanocomposite coatings.

Table 3. Electrodeposition parameters

Deposition Parameters	Values
Plating temperature (℃)	60
Current density (A.dm^{-2})	5
Stirring rate (rpm)	300
pH	7.5
Electrodeposition time (min)	60
Current type	DC
Anode material	Pure Ni (99%)

Apart from the different pretreatment processes used,silicon carbide (SiC) nanoparticle concentration was varied, and its effect on the surface morphology, crystallite structure, microhardness, wear resistance, adhesion, and corrosion resistance were analyzed too. For the studies of the 3D surface contour and roughness of grit blasted and polished specimens ,a Laser scanning confocal microscope (LSCM, OLS4000, OLYMPUS, Tokyo, Japan) was used. A laser scanning confocal microscope (LSCM, OLS4000, OLYMPUS, Tokyo, Japan) was used to analyse the 3D surface contour and roughness of the pretreated 45 steel samples.The coating morphology and microstructure of the deposited coatings was characterized using FEI Quanta FEG 250 scanning electron microscopy (SEM, Hillsboro, OR, USA). SEM coupled with the energy dispersive spectrometer (EDS Oxford max 20, Abingdon, UK) used to determine the composition and the individual elements content of the coatings.

X'Pert Power X-ray Diffraction (XRD, Westborough, MA, USA) with CuK_α radiation, operating at 40 kV and 40mA , scanning from 20° to 90° with the step of 0.02° was used to investigate the predominant crystallographic orientation, phase structure, and grain size of the deposited coatings. Integral peak width was used to determine the average particle size. This can be expressed mathematically using the Debye-Scherrer formula shown in Equation (1).

$$D = \frac{k\lambda}{\beta Cos\theta} . \frac{180℃}{\pi} \quad (1)$$

Where D is the crystallite size, λ represents the X-ray wavelength (0.15406 nm), k the Scherrer constant, β the full width at half maximum (rad), and θ the Bragg angle. The microhardness of the samples was measured using a microhardness tester (Struers, Duramin-40 A1, Ballerup, Copenhagen, Denmark). An applied load of 100 g and an indentation time of 15 s. Ten separate locations were randomly selected for each sample and an average was computed.

Where, F is the applied load and the d is the diagonal of the indentation.

Preprints (www.preprints.org) | NOT PEER-REVIEWED | Posted: 7 June 2021 doi:10.20944/preprints202106.0191.v1

The coating adhesion was measured by a scratch tester. For the measurement of the critical load that the coating could withstand before it was peeled off from the substrate, a load from 0 N to 50 N was gradually applied to the coating.

The friction and wear behaviors of the coating films were evaluated by CFT-1 type material surface performance tester. A loaded GCr15 bearing ball with diameter of 3 mm slid with 4 mm stroke without lubrification over the surface of sample. The load of 320g was applied for a duration of 30 min. Electrochemical corrosion measurements were analyzed by a potentiodynamic polarization test (Tafel) by using an electrochemical workstation comprising of a three-electrode cell in a 3.5 wt.% NaCl medium. The slope of the potential-current density curve defining the polarization resistance Rp was obtained by Stern–Geary equation. It is shown in equation (2) :

$$R_P = \frac{\beta_a \times \beta_c}{2.303 i_{corr}(\beta_a + \beta_c)} \quad (2)$$

Where, β_a is the slope of the anodic Tafel reaction, β_c represents the slope of the cathodic Tafel, reaction and i_{corr} represents the corrosion current density. Electrochemical Impedance Spectroscopy (EIS) experiments were also carried out at the frequencies of 10^5Hz to 10^{-2} Hz at open circuit potential (OCP) where the amplitude of the perturbation voltage was 5mv. Impedance measurements we represented in form of Nyquist and Bode plots.

3. Results

3.1. Surface roughness

Figure 3 shows the surface roughness of the 3D morphology of the samples exposed to the polishing pretreatment and to grit blasting pretreatment. Observing Figure 1a, it can be seen that the surface of the 45 steel subjected to a polishing pre-treatment was smooth without undulations while the grit blasted surface showed large undulations with obvious mountain peak and ravine morphology (Figure 2b). The results show that the grit blasting pretreatment could impart a rough appearance on the 45-steel surface. The surfaces roughness of the polished and grit balsted substrates were evaluated. The Table 3 contains different roughness values (square root roughness Sa and square mean-root roughness Sq) according to the different pretreatments. It can be seen that the values of the square root roughness of the 45 steel having undergone the polishing and grit blasting pretreatment were 0.0047 ± 0.0007µm, and 1.0243 ± 0.3 µm respectively. While the mean square root roughness values were 0.0057 ± 0.0007 µm ,and 1.4237 ± 0.410 µm respectively, suggesting the enhanced effect of grit blasting treatment on the surface roughness. Considering these different results, it appears that the surface roughness could be significantly increased by the use of grit blasting pretreatment. This was found to be in agreement with the results reported in a previous study by the authors [23 , 25–28].

Previous studies have shown that a rough substrate surface was favorable for improving the thickness and adhesion of coatings. Considering the work of Cheng et al. on the adhesion and corrosion resistance of nickel-boron coatings deposited on 8620H alloy Ssteel,

Preprints (www.preprints.org) | NOT PEER-REVIEWED | Posted: 7 June 2021 doi:10.20944/preprints202106.0191.v1

it can be seen that the coating thickness increased with the best adhesion and the best corrosion resistance achieved after the sandblasting pretreatment by emery powders [24].

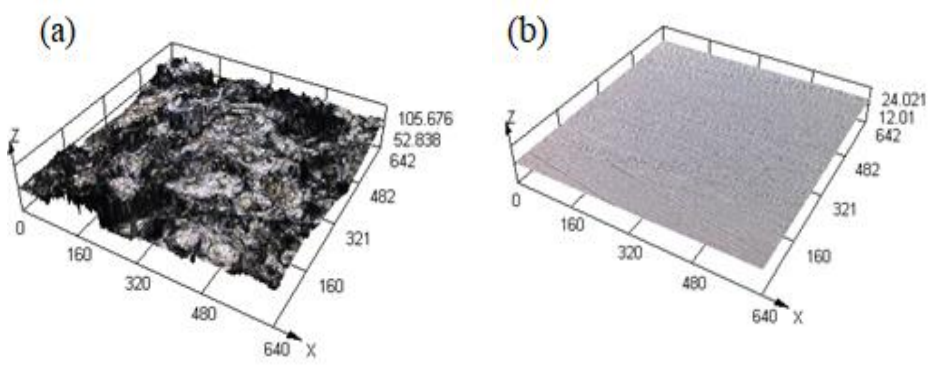

Figure 3. Surface 3D morphology of the substrates subjected to: **(a)** grit blasting and **(b)** polishing.

Table 4. Surface roughness of samples subjected to polishing and grit blasting pretreatment.

Parameters	Polished sample	Grit blasted sample
Sa(μm)	0.0047 ± 0.0007	1.0243 ± 0.3
Sq(μm)	0.0057 ± 0.0007	1.4237 ± 0.410

3.2. Surface morphology

SEM images of the surface morphologies of grit blasted, polished specimens and Ni–W, Ni–W–SiC coatings on 45 steel substrates subjected to two different pretreatments, prepared by conventional electrodeposition images are shown in Figures 4 and 5. From the Figure 4a and the Figure 5a, it can be seen that a large number of random deformations in the form of bulges, flat, and pits were observed on the surface of the grit blasted specimen while the polished surface was flat and smooth with no scratches. Similar result were reported in the previous studies [29,30].

Figure 4b presents the surface microstructure of the Ni–W coating. It shows that the coating had smooth, compact surface. It also exhibited nodular film with developing micro-cracks similar to the surface morphology of Ni–W films studied [31,16].

Ni-W coating pretreated by polishing exhibited a less obvious nodular structure on the surface of the morphology which can be attributed to a lower surface roughness of the 45 steel substrates. Figure 5b shows the surface microstructure of the Ni-W coating subjected to the grit blasting pretreatment, where the cellular structure on the surface of the Ni–W coating was evident. The coating developed on the rough structure of the substrate during deposition and had bumps on the surface. With the presence of numerous bulges, hollows and grain joints with lattice defects generated by grit blasting pretreatment, the surface energy of the defects is relatively low which allowed an easy surmounting of energy barriers to nucleation. The number of nucleation sites then increased because of

Preprints (www.preprints.org) | NOT PEER-REVIEWED | Posted: 7 June 2021 doi:10.20944/preprints202106.0191.v1

defects generated after grit-blasting [32,33]. Thus, the nucleation of the Ni−W alloy is easier after grit-blasting pretreatment.

These different results reveal that with the increase in surface roughness, the number of nucleation points could be increased and the nodules present on the grit blasted surface could become smaller than the ones on polished surface. Similar results were reported by Liu et al. and Vitryn et al. [34,35].

Figure 4c-e and Figure 5c-e present the SEM of Ni–W–SiC coating fabricated on substrate surface subjected to the polishing and grit blasting pretreatments, respectively. From the Figure 4c-e, it is evident that N−W coating's surface morphology was influenced by the SiC nanoparticles. The Ni-W-SiC coatings on the polished substrate show that the addition of SiC nanoparticles in the bath results in a nodular morphology. Moreover, by increasing the SiC concentration, the nodularity increased. A similar morphology was obtained by Ahmadkhaniha et al. [36]. It appears that the increase in SiC nanoparticles further induced the formation of nucleation sites. Other researchers in their studies also observed the nodular morphology[31]. It can be seen that from 3-6 $g.L^{-1}$ of SiC, the morphologies of Ni-W-SiC coatings fabricated on the polished samples had no micro-crack and defects but with 12 $g.L^{-1}$ of SiC the coating morphology contained some defects. Figure 5 c-e showed a formation of more cellular structure on the grit blasted surface. The SiC nanoparticle not only facilitated increasing cathodic polarization and reducing overpotential of metal nucleation of Ni^{2+}, but it also participated in the formation of new crystal nuclei, and prevented aggregation and growth of crystal grains during electroplating, such that the composite coating was refined [37].

The number of nucleation points on the cell structure of the Ni-W-SiC coating was the highest and its size was the smallest with regard to the grit blasted substrate.

Preprints (www.preprints.org) | NOT PEER-REVIEWED | Posted: 7 June 2021 doi:10.20944/preprints202106.0191.v1

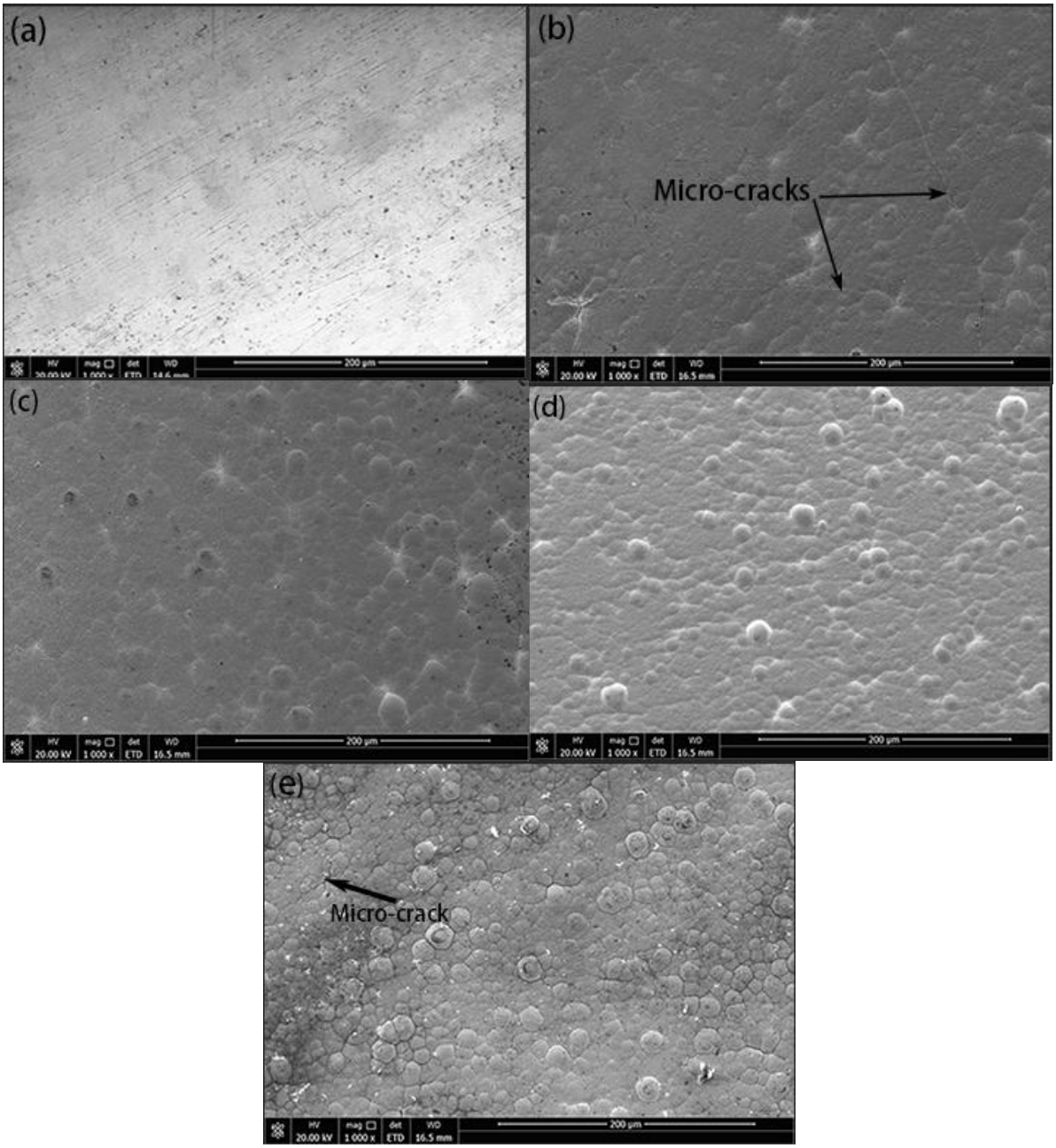

Figure 4. SEM micrographs of (**a**) polished specimen and Ni-W/SiC nanocomposite coatings obtained at different SiC concentration: (**b**) 0 $g.L^{-1}$; (**c**) 3 $g.L^{-1}$; (**d**) 12 $g.L^{-1}$; (**e**)12 $g.L^{-1}$ on polished 45 steel substrate surface.

Preprints (www.preprints.org) | NOT PEER-REVIEWED | Posted: 7 June 2021 doi:10.20944/preprints202106.0191.v1

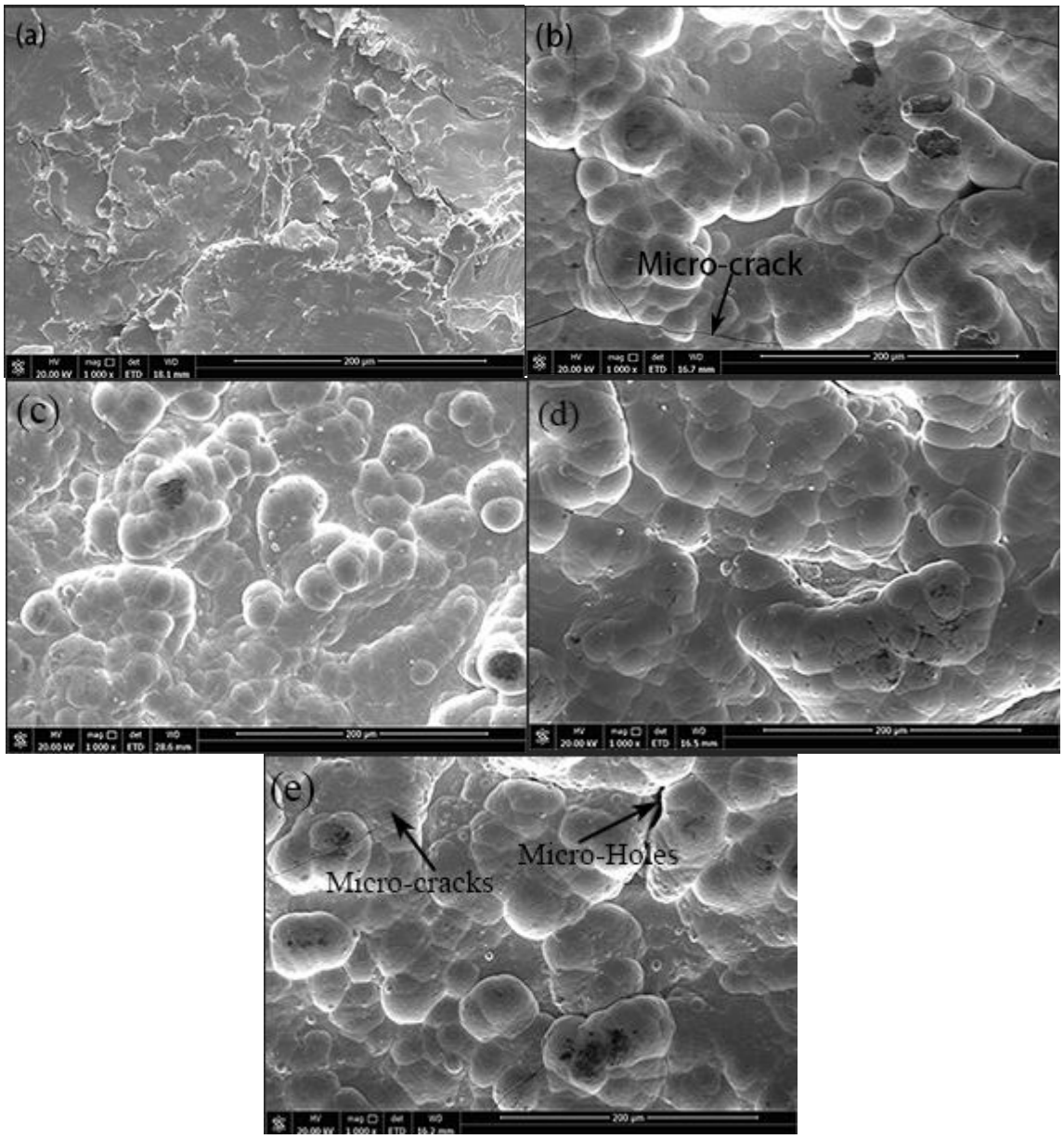

Figure 5. SEM micrographs of (**a**) grit blasted specimen and Ni-W/SiC nanocomposite coatings obtained at different SiC concentration: (**b**) 0 $g.L^{-1}$; (**c**) 3 $g.L^{-1}$; (**d**) 12 $g.L^{-1}$; (**e**)12 $g.L^{-1}$ on grit blasted 45 steel substrate surface.

3.3. Cross-sectional microstructure and EDS

Figure 6 and Figure 7 show the cross sectional structure of Ni–W and Ni-W/SiC nanocomposite coatings deposited on the polished and grit blasted 45 steel, respectively. The cross-sectional morphology of the Ni–W coating on the polished substrate is shown in Figure 6a. The coating was a uniform deposit on the surface of the smooth substrate with a thickness of about 17.35 ± 0.39 μm. Figure 7a presents the cross-sectional morphology of the Ni-W coating on the grit blasted substrate. There existed a tight bond between the coating and the rough surface of the substrate and the formation of a mechanical interlock resulting from the filling of the holes in the substrate. The thickness is approximately 18.45 ± 0.53 μm, with pits up to 26.27 μm. Cheng et al. demonstrated that the increase in thickness observed is due to the high surface roughness caused by grit blasting which increased the number of nucleation points in the coating. Figure 6b-d shows cross sections

Preprints (www.preprints.org) | NOT PEER-REVIEWED | Posted: 7 June 2021 doi:10.20944/preprints202106.0191.v1

of the Ni–W/SiC nanocomposite deposited on the polished 45 steel with the variation of the SiC nanoparticle concentration. With the increase of SiC particles from 3 $g.L^{-1}$ to 12$g.L^{-1}$ the coatings exhibited a more compact cross section with good adhesion of the coating matrices to the substrate surface and the coating thickness increased. to 29.97 ± 0.49 µm at 6$g.L^{-1}$ before decreasing to 20.95 ± 0.88 at 12$g.L^{-1}$. Similar change in thickness as a function of the variation in the SiC concentration shown in Figure 8a was reported in a previous research [38]. Compared to the Ni–W coating, the thickness of all the Ni-W-SiC coatings were increased. This is due to the fact that the SiC particles refined the microstructure of the Ni-W coating and promoted its growth [37, 39].

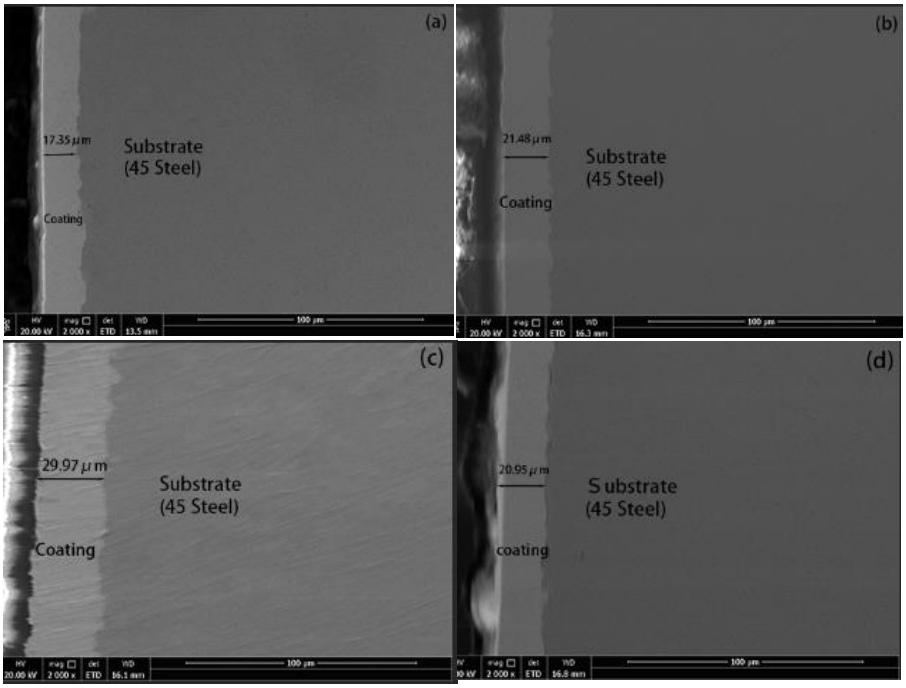

Figure 6: SEM micrographs illustrating coating cross section of Ni-W/SiC nanocomposite coatings obtained at different SiC concentration: (**a**) 0 $g.L^{-1}$; (**b**) 3 $g.L^{-1}$; (**c**) 12 $g.L^{-1}$; (**d**)12 $g.L^{-1}$ on polished 45 steel substrate surface

Figure 6b-d shows cross sections of the Ni–W/SiC coatings with the variation of the SiC nanoparticle concentration and deposited on the grit-blasted 45-steel. With the increase of SiC particles from 3 g/L^{-1} to 12 g/L^{-1} the coating thickness increased to 25.9 ± 1.5 µm at 6 g/L^{-1} before decreasing to 21.47 ± 0.63 µm at 12 g/L^{-1} Compared with the Ni–W coating, the thickness of all the Ni-W-SiC coatings were increased. The change in thickness as a function of the variation in the SiC concentration is shown in Figure 8b. The high adhesion to the rough substrate was due to the effect of the SiC nanoparticles. In addition, the valleys and apparent peaks appear on the surface of the substrate which would have caused the densification of the nodular structure observed on the morphological surface shown in Figure 5 c-e [24].

Preprints (www.preprints.org) | NOT PEER-REVIEWED | Posted: 7 June 2021 doi:10.20944/preprints202106.0191.v1

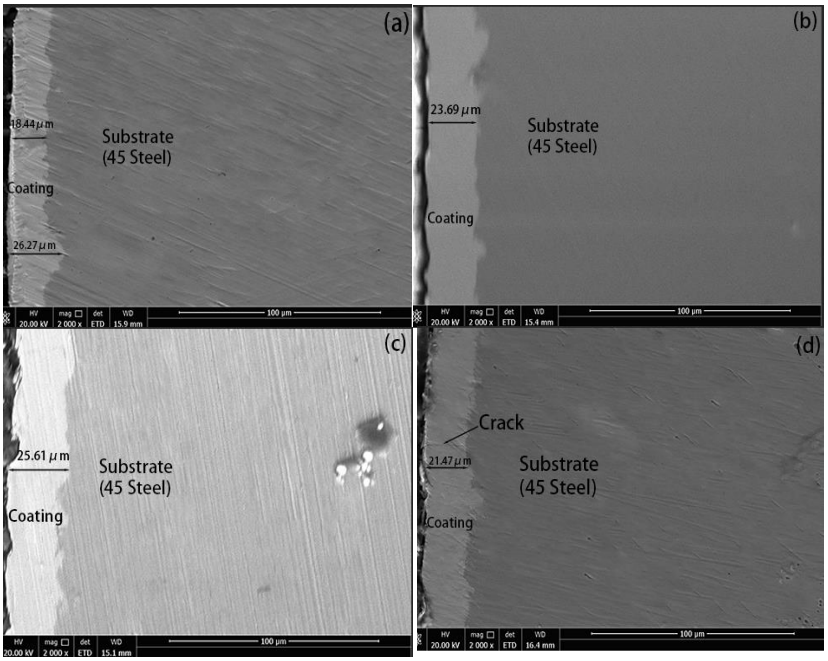

Figure 7: SEM micrographs illustrating coating cross section of Ni-W/SiC nanocomposite coatings obtained at different SiC concentration: (**a**) 0 g.L^{-1}; (**b**) 3 g.L^{-1}; (**c**) 12 g.L^{-1}; (**d**)12 g.L^{-1} on grit blasted 45 steel substrate surface.

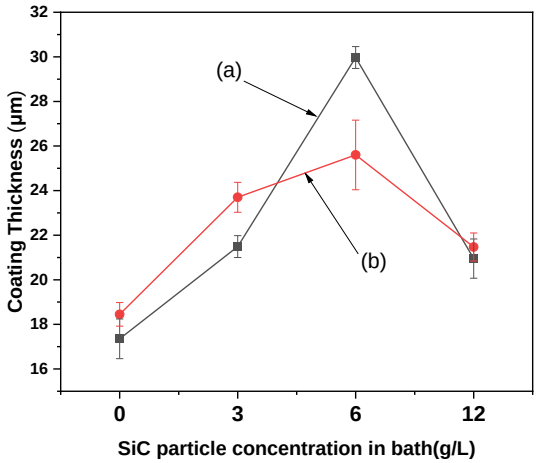

Figure 8. Thickness for different Ni-W- SiC composite coatings fabricated on (**a**) polished and (**b**) grit blasted 45 steel obtained at different SiC concentrations.

Figure 9. presents the EDS spectrum of the Ni–W Coatings pretreated by polishing : Ni–W(P), pretreated by grit blasting : Ni–W(GB) and Ni–W–SiC nanocomposite coatings pretreated by polishing : Ni-W–SiC(P) and grit blasting pretreated : Ni-W–SiC(GB). As can be seen in Figure 9a,b, the EDS spectra of Ni–W coatings prepared under the different processes present the peaks of Ni and W, where the Si and C content were not found. As can be seen in Figure 9c,d besides Ni peaks, peaks corresponding to W and Si, C are also visible in the all cases. That is, the SiC particles were successfully co-deposited in Ni–W coatings. With polishing or gritblasting pretreatments, the incorporation of SiC into Ni-W reduced the amount of Ni and W. For Gyawali et al. [40] the decrease in Ni and W in the coating during the codeposition of SiC nanoparticles can be explained in terms of

Preprints (www.preprints.org) | NOT PEER-REVIEWED | Posted: 7 June 2021 doi:10.20944/preprints202106.0191.v1

Faraday's efficiency. According to Figure 9c,d, Ni–W–SiC(P) (6 g.L^{-1} of SiC) coating has lesser content of W (31.6 wt·%) as compared to Ni–W-SiC(GB) (6 g.L^{-1} of SiC),(35.48wt·%). Moreover the SiC content in all cases was low.

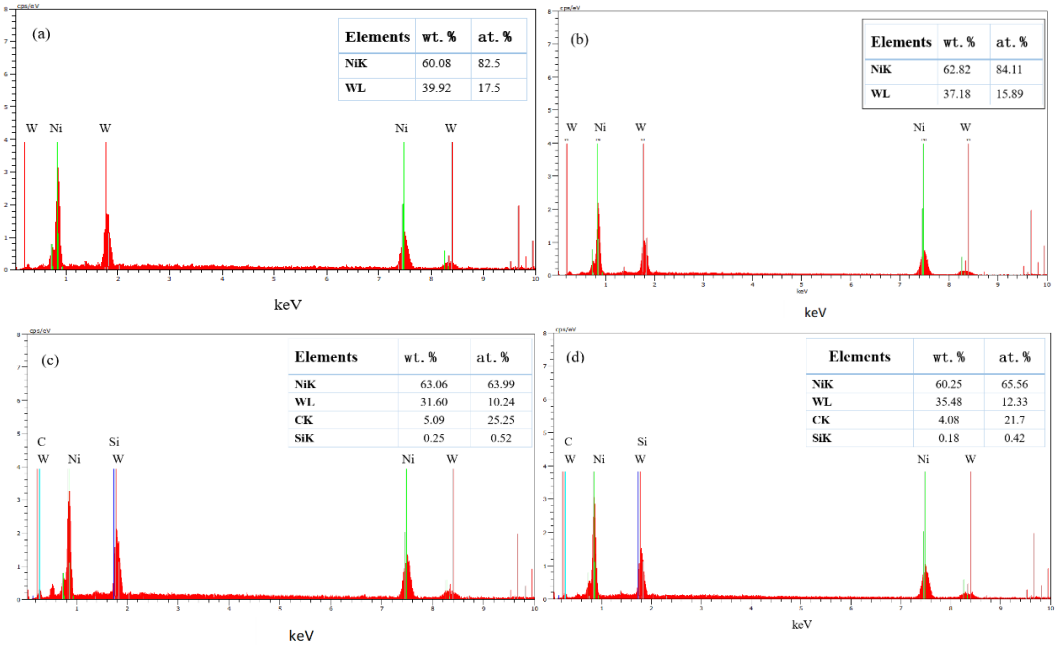

Figure 9. EDS spectra of: (**a**) Ni–W(P), (**b**) Ni–W(G), (**c**) Ni–W–SiC(P), (**d**) Ni–W–SiC (GP).

3.4. XRD Analysis

Figure 11 and Figure 12 show the XRD patterns of Ni–W and Ni–W–SiC composite coatings on the polished and grit-blasted samples, respectively. In this study all the coatings have shown a face-centered cubic structure. where in the polished sample, the peaks at 2θ equal to 43.72, 50.94, 74.76 are associated with (111), (200) and (220) Ni peaks, respectively while in the case of grit-blasted samples, the peaks at 2θ located to 43.55, 50.83, 74.57 are associated with (111), (200) and (220) Ni peaks planes, respectively. The lattice parameters of the Ni-W solid solution being larger than those of pure Ni coating. It had beennoticed in the literature that the diffraction peaks of the Ni-W solid solution were shifted towards lower values 2θ compared to the positions of pure Ni [20]. With the increase of SiC, the preferred orientation of Ni-W-SiC coatings did not change significantly. For both grit blasting and polishing processes. The XRD results presented in Figure 11 and Figure 12 show that the peaks corresponding to the SiC nanoparticles were not detected on the XRD pattern of the nanocomposite coatings but was confirmed by the EDS analysis. This was due to the low reinforcement content of the SiC nanoparticle in the deposited composite [40]. The crystallite size of Ni-W alloy coating and of Ni-W-SiC composite coatings was calculated using the Scherer's equation and the grain values for the various electrodeposits are shown in the Figure 13. The crystallite grain size of Ni-W-SiC nanocomposite was observed to decrease as compared to Ni-W coating for the all pretreatments process.

As shown in Figure 13a, the grain size of Ni-W-SiC coatings obtained in the case of polishing pretreatment process (a) from plating bath with different SiC nanoparticle

Preprints (www.preprints.org) | NOT PEER-REVIEWED | Posted: 7 June 2021 doi:10.20944/preprints202106.0191.v1

concentration decreased with the increase of SiC concentration from 8.97nm at 0 $g.L^{-1}$ to 8.16 nm at 6 $g.L^{-1}$ beyond which it increased to 8.7nm at 12 $g.L^{-1}$. Concerning the grit blasting pretreatment (Figure 13b) the grain size of Ni-W-SiC coatings obtained from plating bath with the different SiC nanoparticle concentration decreased with the increase of SiC concentration from 8.21 nm at 0 $g.L^{-1}$ to 6.76 nm at 6 $g.L^{-1}$ beyond which it increased to 7.37 nm at 12 $g.L^{-1}$. Similar trend was confirmed in previous publications [41–43]. From the result, the smallest grain size for both pretreatment processes was obtained at 6 $g.L^{-1}$. According to the theory of electrodeposition, the nucleation rate and the rate of grain growth are the main basis for determining grain size. This is because the faster the nucleation rate, the slower the grain growth rate and the smaller the grains. The SiC nanoparticles added were absorbed at the cathode surface and created a large nucleation growth site favorable for coatings. The SiC nanoparticles were embedded in the metal grain boundaries of the Ni-W matrix and inhibited the growth of the grains, thereby reducing the size.

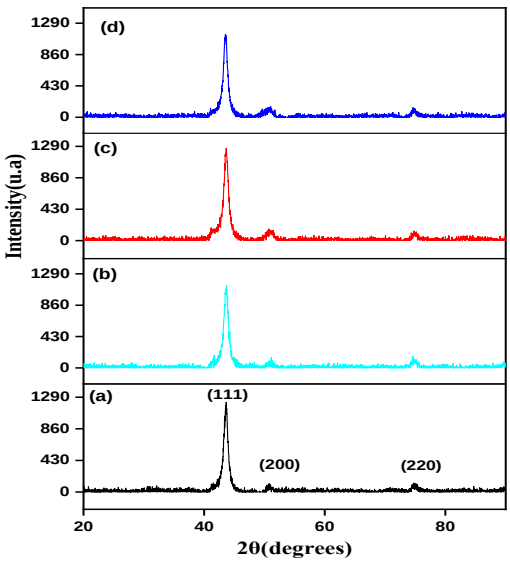

Figure 11. XRD patterns of Ni-W-SiC composite coatings on polished 45 steel obtained at different SiC concentration: (**a**) 0 $g.L^{-1}$; (**b**) 3 $g.L^{-1}$; (**c**) 12 $g.L^{-1}$; (**d**)12 $g.L^{-1}$.

Preprints (www.preprints.org) | NOT PEER-REVIEWED | Posted: 7 June 2021 doi:10.20944/preprints202106.0191.v1

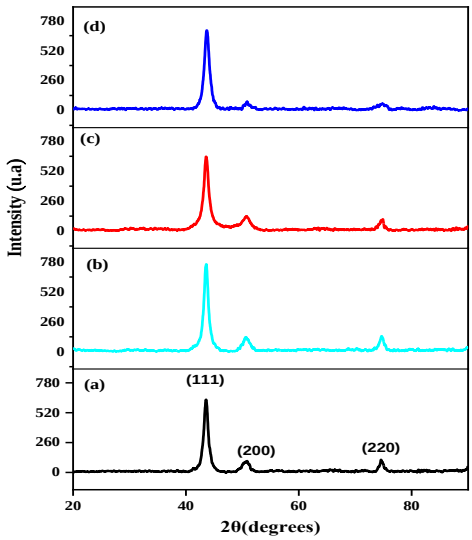

Figure 12. XRD patterns of Ni-W-SiC composite coatings on grit blasted 45 steel obtained at different SiC concentration: (**a**) 0 g.L^{-1}; (**b**) 3 g.L^{-1}; (**c**) 12 g.L^{-1}; (**d**)12 g.L$^{-1.}$

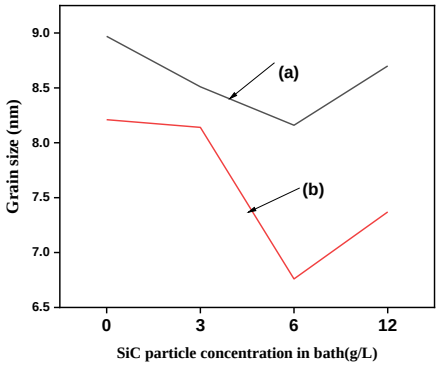

Figure 13. Grain sizes for different Ni-W- SiC composite coatings fabricated on (**a**) polished and (**b**) grit blasted 45 steel obtained at different SiC concentration.

3.5. Microhardness

For objects subjected to a wear environment, two important properties of wear resistance and hardness are essential. Figure 14 presents the microhardness of the Ni–W–SiC nanocomposite coatings on the **(a**) polished and (**b**) gritblasted 45 steel as a function of SiC concentration. It was noted that for the grit blasting or polishing pretreatments processes, the microhardness increased with the increase in the concentration of SiC such that the microhardness of all Ni–W/SiC nanocomposites coating were higher than that of Ni–W coating alloy. Without SiC, the deposited Ni–W exhibited the hardness for polishing and grit blasting of 550.25 ± 7.04 Hv and 589.89 ± 10 Hv, respectively. The presence of SiC in the Ni–W coatings considerably increased the microhardness for all pretreatment processes. It is clear that an increase in the amount of SiC particle codeposition led to an increase in the hardness of the coatings. With an increase in the SiC concentration from 3 to 6 g.L^{-1}, the microhardness increased for the polishing and gritblasting processes to 639.12 ± 5.76 Hv and 673 ± 5.47Hv, respectively before decreasing when concentration of SiC was increased from 6 to 12 g.L^{-1}. This effect of the nanoparticle on the coatings alloys has been

Preprints (www.preprints.org) | NOT PEER-REVIEWED | Posted: 7 June 2021 doi:10.20944/preprints202106.0191.v1

described in the previous researches [15, 44–46]. One possible reason for this result is that the SiC nanoparticles in the Ni–W–SiC coating blocked the dislocation movement and sliding at the grain boundary of the matrix, thereby increasing the micro-hardness of the Ni–W–SiC. The alloy matrix strengthening mechanism is mainly due to grain refinement, particle strengthening and dispersion hardening effects [42]. The higest hardness was obtained with the nanocomposite with the lowest grain size of 6.76 nm. This is in agreement with the Hall-Petch [47] formula which states that the smaller the particle size, the higher the hardness of the nickel matrix.

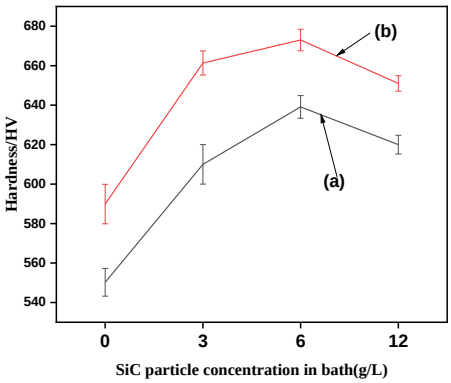

Figure 14. Presents the microhardness values for of Ni–W and Ni–W–SiC coatings on 45 steel substrates subjected to (**a**) polishing and (**b**) grit blasting pretreatments by varying the SiC concentration in the electrolyte

3.6. Coating adhesion

Figure 15 shows the adhesion of the coatings prepared on 45 steel substrates by electrodeposition with different pretreatment processes and by varying the SiC concentration. One of the important factors that degrades the protective performance and corrosion process of coatings is adhesion. Therefore poor adhesion can cause performance failure of Ni–W–SiC coatings. It was found that the adhesion of Ni-W alloys was not deteriorated by nanoparticles in any case whether the substrate was pretreated by polishing or by grit blasting. The addition of SiC inhibited the growth of Ni-W grain, and the grain size of the coating was refined. The effective contact area between the coating and the substrate increased and based on the mechanism of the dispersal reinforcement of the nanoparticles, the adhesion of the coatings improved [48].

The adhesion of the Ni–W alloy coating on the polished and grit blasted substrates was 11.25 N and 14.25 respectively.Ni–W coating adhesion of the polished substrate was lower than that of the grit blasted substrate. This remark is due to the rough surface obtained after blasting which leads to the extrusion of the protrusions in the scratches. Fu et al. [27] studied the influence of the region of penetration elements on the adhesion and corrosion performance of the Ni-based coatings and indicated pre-processing by sanding increased the effective contact surface between the substrate and the coating and participated in the widening of the area of penetration of the element which led to improved adhesion of the

Preprints (www.preprints.org) | NOT PEER-REVIEWED | Posted: 7 June 2021 doi:10.20944/preprints202106.0191.v1

coating. Morever Cheng et al. [24] found that, the high surface roughness of the surfaces provided the higher adhesion force. Whether in polishing or grit blasting pretreatment, with the addition of the nano-SiC particles from 3-6g.L^{-1}, the adhesion of the composite coatings gradually increased before decreasing when the nano-SiC concentration was from 6 to 12 g.L^{-1} . After the polishing pretreatment, the adhesion of the Ni - W - SiC coating increased to 26 ± 0.5N (SiC of6g.L^{-1}) before decreasing to 13 N (12 g.L^{-1} of SiC). This effect of SiC nano-particles was confirmed by the previous studies [37,44]. Adhesion obtained after grit blasting pretreatment increased to 33 ± 0.75 N (6 g.L^{-1} of SiC) before decreasing to 28 ± 1 N (12 g.L^{-1} of SiC). This indicates the improvement in the interface bond strength between the coating and the metal substrate. This may be due to the high hardness of the SiC nanoparticles which played a major role in the coupling of the matrix [20]. It should be noted that the fact that the size of the Ni-W crystal is much larger than those of the SiC nanoparticles, the SiC nanoparticles could fill the pores between the grains of Ni-W deposits, which could participate in the reduction of the porosity and improving the compactness of the coating. The metal matrix with a fine grain had a relatively high yield strength, according to the Hall-Petch equation [49,50]. The finer the size of the grain the larger the grain limit and this hinders the dislocation movement. Thus, the accumulation of dislocation at the boundary of the grain led to increase in the strength of the coating. This remark is confirmed with the Figure 13,17. In this study, the coatings with the small grain size had better coating adhesion for both polishing and grit blasting pretreatment.

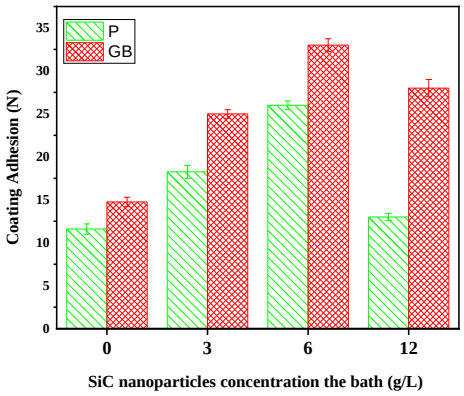

Figure 15. The analysis of critical load of Ni-W and Ni-W- SiC composite coatings on 45 steel substrates subjected to grit blasting pretreatment by varying the SiC concentration in the electrolyte.

Preprints (www.preprints.org) | NOT PEER-REVIEWED | Posted: 7 June 2021 doi:10.20944/preprints202106.0191.v1

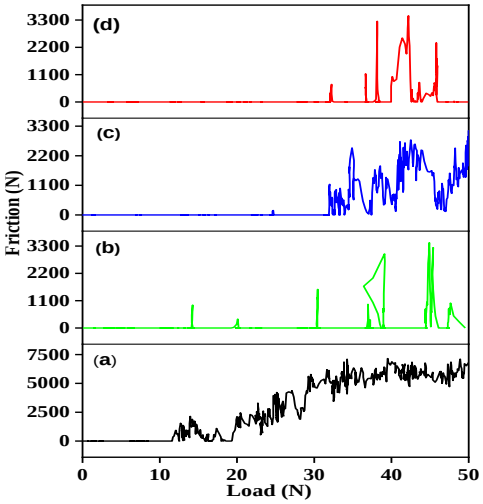

Figure 16. Shows the adhesion strength test curves measured by scratch tester: (a) Ni-W(P), (b) Ni W(GP), (c)Ni-W-6SiC(P), (d) Ni-W-6SiC (GB).

3.6. Corrosion Resistance

Figure 18 shows the polarization curves of coatings fabricated on 45 steel substrates subjected to the different pretreatment processes. Extrapolation method was to determine the corrosion potential (E_{corr}), corrosion current density (i_{corr}), the polarization resistance (R_P) and corrosion rate (r_{corr}) as shown in Table 5. The results show that compared to polished samples, the corrosion potential of the grit-blasted substrate increased from -957 to - 830 mV, and the polarization resistance increased from -957 to - 830 mV, implying pre-treatment by grit blasting improved significantly the substrate's surface corrosion resistance. This is because after pre-processing by grit blasting a rough structure was generated and after the infiltration of corrosion products, they could not be easily diffused. Similar results are found by Fu et al. and Zhang et al. [27,30]. Compared with the base substrate, it was found that the corrosion potential of the Ni-W coating was significantly greater than that of the substrate. In addition, the polarization resistance of the Ni-W coating far exceeded that of the substrate and the corrosion rate decreased too. This result shows that the Ni-W coating was an effective protection against corrosion of the exposed base substrate. Moreover, compared with the polishing pretreatment, the Ni-W(GB) coating alloy exhibited -696 mV (-744 mV for polishing) as the potential corrosion and 11.4 $k\Omega.cm^{-2}$ as polarization resistance value and 2.13 $k\Omega.cm^{-2}$ for Ni-W(P) . For Fu et al. [27] this positive effect of the Ni-W coating can be explained by the fact that there was the formation of the region of penetration of the elements between the Ni-W coating and the base substrate. This led to a second layer formation at the substrate for corrosion protection. Additionally,the increased adhesion of the coating caused by the application of the grit blasting is one of the factors that contributed to the improvement in the corrosion resistance of the coating. For both polishing and sandblasting, there was an increase in the corrosion potential and in the polarization resistance of the Ni - W - SiC nano composite coating compared to the Ni-W alloy coating. The Ni–W–6SiC(GB) nanocomposite coating exhibited the highest corrosion potential Ecorr(-560mv) and the highest corrosion

Preprints (www.preprints.org) | NOT PEER-REVIEWED | Posted: 7 June 2021 doi:10.20944/preprints202106.0191.v1

resistance Rp (12.7 kΩ.cm^{-2}) compared to Ni–W–6SiC(P) nanocomposite coating. The EDS showed that the SiC particles were evenly distributed over the Ni-W-SiC nanocomposite which resulted in the refining of the coating structure, and the creation of an area which reduced the infiltration of corrosion products.

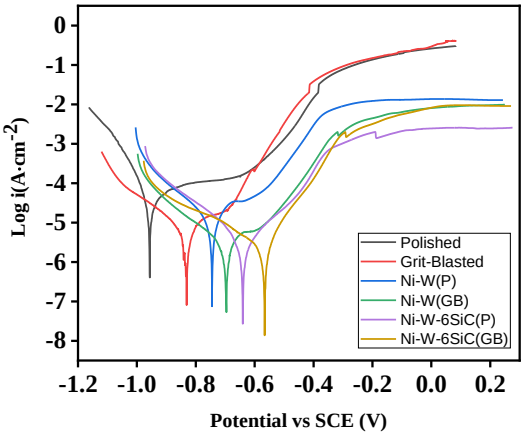

Figure 17. Polarization curves of coatings prepared by scanning electrodeposition on 45 steel substrates with different pretreatment processes.

Table 5. Electrochemical data from potentiodynamic polarization curves of the polished, grit- blasted specimens and Ni–W-SiC coating on polished and grit blasted 45 steels as a function of SiC nan particles concentration in the electrolyte.

Specimens	E_{corr} (mV_{SCE})	i_{corr} ($\mu A.cm^{-2}$)	r_{corr} (mmPY)	β_a ($mV.dec^{-1}$)	β_b ($mV.dec^{-1}$)	R_p ($k\Omega.cm^{-2}$)
polished	-957	29	0.57	523.04	88.97	1.13
Grit-Blasted	-830	27.86	0.243	1212.5	429.82	4.95
Ni-W(P)	-744	19.3	0.17	181.42	193.01	2.13
Ni-W(GB)	-696	14.12	0.12	1507.7	489.62	11.4
Ni-W-6SiC(P)	-640	5.15	0.05	219.72	189.2	8.57
Ni-W-6SiC (GB)	-560	3.71	0.03	155.2	357.24	12.7

For supporting the findings from the potentiodynamic polarization an additional corrosion resistance study of the Ni-W and Ni-W-SiC coating under the different pretreatment processes was done by using a non-destructive electrochemical impedance spectroscopy (EIS) method to study the behavior of each sample in 3.5 wt % NaCl solution. Figure 19 depicts the Nyquist plots and Bode plots recorded for the Ni-W and Ni-W-SiC coatings pretreated by the different processes. The increase in the impedance arc radius indicates that the coating had a better resistance to corrosion. The Nyquist were fitted using the ZSimpWin software, the results are listed in Table 6. The figure shows the equivalent electrical circuit, in which the Rs was the electrolyte resistance, CPEdl was the

Preprints (www.preprints.org) | NOT PEER-REVIEWED | Posted: 7 June 2021 doi:10.20944/preprints202106.0191.v1

constant phase element and Rct represented the capacitive behavior at the interfaces of coating/substrate. The results show that the grit-blasted substrate, effectively improved the corrosion resistance seeing that after grit blasting ,the Rct value increased from 0.665 to 0.940 kΩ.cm^{-2} . The 45 steel had the smallest capacitive radius and thus, the lowest corrosion resistance Meanwhile, the Ni-W-6SiC(P) nanocoatings had a capacitive arc radius larger than the Ni-W(P). In addition, Ni–W–6SiC(GB) nanocomposite coating with Rct value, reaching 4.92 kΩ.cm^{-2} had the largest capacitive arc radius and had the highest corrosion resistance. The results of the EIS and the corrosion resistance obtained in the polarization curve had a similar trend. The Ni-W-SiC composite coating pre-treatment by grit blasting had best corrosion resistance.

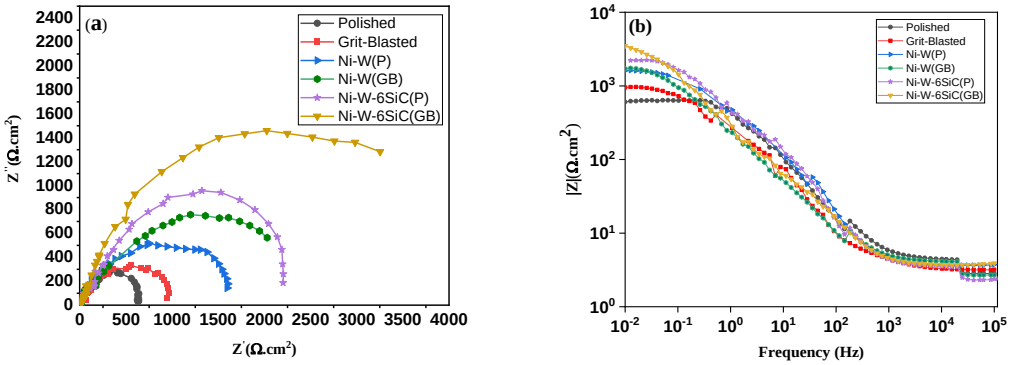

Figure 18. Electrochemical impedance spectra for Ni-W and Ni-W-SiC coatings 45 steel substrates subjected to two different pretreatments in 3.5 NaCl: (**a**) Nyquist plots; (**b**) Bode plots.

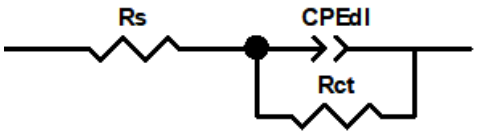

Figure 19. Equivalent circuit for Nyquist plots analysis.

Table 6. The equivalent circuit parameters and Fitting results of the impedance spectra of Ni-W and Ni-W-SiC coatings pretreated by two different processes.

Specimens	Rs(Ω.cm^{-2})	CPE-T(10^{-5}.F. cm^{-2})	CPE-P	Rct(kΩ.cm^{-2})
polished	3.72	34.95	0.79	0.665
Grit-Blasted	3.14	68.04	0.77	0.940
Ni-W(P)	3.40	25	0.85	1.49
Ni-W(GB)	3.408	42.3	0.70	2.27
Ni-W-6SiC(P)	2.69	37	0.78	2.21

 doi:10.20944/preprints202106.0191.v1

Ni-W-6SiC (GB)	3.427	86.6	0.703	4.92

4. *Conclusions*

In this work, Ni-W coating and Ni-W-SiC nanoparticles coating were fabricated on 45 steel substrates pretreated by polishing and sandblasting in order to study the effects of roughness and SiC nanoparticles on the microhardness, adhesion strength and corrosion resistance on the coatings. It can be concluded that, Grit blasting and SiC nanoparticles significantly strengthened the adhesion between the coating and the substrate. Meanwhile, the microhardness and the corrosion resistance improved.

(1) The Ni–W–SiC (6 $g.L^{-1}$ of SiC) nanocomposite fabricated on the grit blasted 45 Steel substrates exhibited the highest hardness compared to the one fabricated on polished 45 substrates.

(2) The adhesion of the Ni-W-SiC (6 $g.L^{-1}$) nanocomposite coating pretreated by grit blasting was 33± 0.75 N, which was higher than the one pretreated by polishing.

(3) The Ni–W–SiC (6 $g.L^{-1}$ of SiC) nanocomposite fabricated on the grit blasted 45 Steel substrates exhibited the highest corrosion resistance compared to the one fabricated on polished 45 substrates.

Author Contributions: Conceptualization, G.V.B. and M.K.; methodology, G.V.B. and S.M.N; software, G.V.B., A. E. and Y.Z; validation, G.V.B., M.K. and N. J.N.; formal analysis, G.V.B. and N. J.N.; investigation, G.V.B., A.E and S. M.N. ; resources, M.K.; data curation, G.V.B., N.J.N. and A.E; writing—original draft preparation, G.V.B. and S.M.N; writing—review and editing, G.V .B. and M.K.; visualization, G.V.B., A.E and N. J.N; supervision, M.K.; project administration, M.K and Y.Z; funding acquisition, M.K.

Funding: The research was funded by Jiangsu Key Research and development program, Grant No. BE2020311

Conflicts of Interest: The authors declare no conflict of interest.

References

1 Paczkowska, M.; Selech, J.; Piasecki, A. Effect of Surface Treatment on Abrasive Wear Resistance of Seeder Coulter Flap. Surf. Rev. Lett. **2016**, 23 , 1–11. https://doi.org/10.1142/S0218625X16500074.

2 Cooke, K. O. Tribological Performance of Hardfaced / Thermally Sprayed Coatings for Increased Wear Resistance of Cutting Blades Used in Harvesting Sugarcane. Ann. Agric. Crop Sci. **2019**, 4 , 1–7.

3 Refai, M.; Hamid, Z. A.; El-Kilani, R. M.; Nasr, G. E. M. Reducing the Wear and Corrosion of the Agricultural Machinery by Electrodeposition Nanocomposite Coatings-Review.Egypt.J.Chem.**2020**, 63,3075–3095. https://doi.org/10.21608/EJCHEM.2020.28677.2615.

4 Clara, S.; Clara, V. Performance of the Base-Cutter Blades in the Sugarcane Harvester Machines Case-IH 7000. Rev. Ciencias Técnicas Agropecu. **2018**, 27 , 1–9.

5 Niranatlumpong, P.; Sukhonket, C.; Nakngoenthong, J. Wear Resistant Surface Treatment of Pulverizer Blades. Wear **2013**, 302 , 878–881. https://doi.org/10.1016/j.wear.2012.11.078.

6 Kenneth Holmberg, A. M. Chapter 2 Surface Coating Methods. In Tribology Series; 1994; 28, 7–32. https://doi.org/10.1016/S0167-8922(08)70752-1.

7 Fotovvati, B.; Namdari, N.; Dehghanghadikolaei, A. On Coating Techniques for Surface Protection: A Review. J. Manuf. Mater. Process. **2019**, 3 , 28. https://doi.org/10.3390/jmmp3010028.

8 Singh, S.; Garg, J.; Singh, P.; Singh, G.; Kumar, K.; Singh, J.; Kumar, S.; Singh, J. P. Effect of Hard Faced Cr-Alloy on Abrasive Wear of Low Carbon Rotavator Blades Using Design of Experiments. Mater. Today Proc. **2018**, 5 , 3390–3395.

https://doi.org/10.1016/j.matpr.2017.11.583.

`9 Chen, H.; Ren, X. R.; Zhang, X. H.; Li, J. H. Wear and Corrosion Properties of Crystalline Ni-W Alloy Coatings Prepared by Electrodeposition. Mater. Sci. **2016**, 849, 671–676. https://doi.org/10.4028/www.scientific.net/MSF.849.671.

10 Hu, Y.; Yu, Y.; Ge, H.; Wei, G.; Jiang, L. Study on Mechanical and Anticorrosion Performance of NiW Alloy Coatings Prepared by Induced Codeposition. Int. J. Electrochem. Sci. **2019**, 14 , 1649–1657. https://doi.org/10.20964/2019.02.19.

11 Elias, L.; Hegde, A. C. Effect of Magnetic Field on Corrosion Protection Efficacy of Ni-W Alloy Coatings. J. Alloys Compd. **2017**, 712, 618–626. https://doi.org/10.1016/j.jallcom.2017.04.132.

12 Pramod Kumar, U.; Liang, T.; Kennady, C. J.; Nandha Kumar, R.; Prabhu, J. Influence of Positional Isomeric Spacers of Naphthalene Derivatives on Ni–W Alloy Electrodeposition: Electrochemical and Microstructural Properties. ACS Omega **2020**, 5 , 3376–3388. https://doi.org/10.1021/acsomega.9b03599.

13 Wasekar, N. P.; Latha, S. M.; Ramakrishna, M.; Rao, D. S.; Sundararajan, G. Pulsed Electrodeposition and Mechanical Properties of Ni-W/SiC Nano-Composite Coatings. Mater. Des. **2016**, 112, 140–150. https://doi.org/10.1016/j.matdes.2016.09.070.

14 Zhang, W.; Ji, C.; Li, B. Synthesis and Properties of Ni–W/ZrO2 Nanocomposite Coating Fabricated by Pulse Electrodeposition. Results Phys. **2019**, 13 , 102242. https://doi.org/10.1016/j.rinp.2019.102242.

15 Li, B.; Zhang, W. Microstructural, Surface and Electrochemical Properties of Pulse Electrodeposited Ni–W/Si3N4 Nanocomposite Coating. Ceram. Int. **2018**, 44, 19907–19918. https://doi.org/10.1016/j.ceramint.2018.07.254.

16 Allahyarzadeh, M. H.; Aliofkhazraei, M.; Rouhaghdam, A. R. S.; Torabinejad, V. Electrodeposition of Ni–W–Al2O3 Nanocomposite Coating with Functionally Graded Microstructure. J. Alloys Compd. **2016**, 666, 217–226. https://doi.org/10.1016/j.jallcom.2016.01.031.

17 Lai, G.; Liu, H.; Chen, B.; Niu, D.; Lei, B.; Jiang, W. Electrodeposition of Functionally Graded Ni-W/Er2O3 Rare Earth Nanoparticle Composite Film. Int. J. Miner. Metall. Mater. **2020**, 27, 818–829. https://doi.org/10.1007/s12613-019-1953-z.

18 Moein, A.; Rastegari, S. Effect of Pulse Parameters on the Morphology of Electroplated Ni–W–TiC Nanocomposite Coating. Surf. Eng. **2020**, 36 , 982–989. https://doi.org/10.1080/02670844.2019.1708569.

19 Hosseini, M. G.; Abdolmaleki, M.; Ghahremani, J. Investigation of Corrosion Resistance of Electrodeposited Ni-W/SiC Composite Coatings. Corros. Eng. Sci. Technol. **2014**, 49, 247–253. https://doi.org/10.1179/1743278213Y.0000000120.

20 Bin Humam, S.; Gyawali, G.; Dhakal, D. R.; Choi, J. H.; Lee, S. W. Effect of Pulse and Direct Current Electrodeposition on Microstructure, Surface, and Scratch Resistance Properties of Ni–W Alloy and Ni–W–SiC Composite Coatings. Acta Metall. Sin. (English Lett. **2020**, 33 , 1321–1330. https://doi.org/10.1007/s40195-020-01098-w.

21 Li, B.; Zhang, W.; Zhang, W.; Huan, Y. Preparation of Ni-W/SiC Nanocomposite Coatings by Electrochemical Deposition. J. Alloys Compd. **2017**, 702, 38–50. https://doi.org/10.1016/j.jallcom.2017.01.239.

22 Ziemian, C. W.; Sharma, M. M.; Bouffard, B. D.; Nissley, T.; Eden, T. J. Effect of Substrate Surface Roughening and Cold Spray Coating on the Fatigue Life of AA2024 Specimens. Mater. Des. **2014**, 54, 212–221. https://doi.org/10.1016/j.matdes.2013.08.061.

23 Li, D.; Wu, J.; Miao, B.; Zhao, X.; Mao, C.; Wei, W.; Hu, J. Enhancement of Wear Resistance by Sand Blasting-Assisted Rapid Plasma Nitriding for 304 Austenitic Stainless Steel. Surf. Eng. **2020**, 36, 524–530. https://doi.org/10.1080/02670844.2019.1641953.

24 Cheng, A. Y.; Sheu, H. H.; Liu, Y. M.; Hou, K. H.; Hsieh, P. Y.; Ger, M. Der. Effect of Pretreatment Process on the Adhesion and Corrosion Resistance of Nickel-Boron Coatings Deposited on 8620H Alloy Steel. Int. J. Electrochem. Sci. **2020**, 15 , 68–79. https://doi.org/10.20964/2020.01.22.

25 Amiriafshar, M.; Rafieazad, M.; Duan, X.; Nasiri, A. Fabrication and Coating Adhesion Study of Superhydrophobic Stainless Steel Surfaces: The Effect of Substrate Surface Roughness. Surfaces and Interfaces **2020**, 20 , 100526. https://doi.org/10.1016/j.surfin.2020.100526.

26 Arifvianto, B.; Suyitno; Mahardika, M. Effect of Sandblasting and Surface Mechanical Attrition Treatment on Surface Roughness, Wettability, and Microhardness Distribution of AISI 316L. Key Eng. Mater. **2011**, 462–463, 738–743. https://doi.org/10.4028/www.scientific.net/KEM.462-463.738.

27 Fu, X.; Shen, Z.; Chen, X.; Lin, J.; Cao, H. Influence of Element Penetration Region on Adhesion and Corrosion Performance of Ni-Base Coatings. Coatings **2020**, 10. https://doi.org/10.3390/COATINGS10090895.

28 HAMMOUDA, N.; BELMOKRE, K. Effect of Surface Treatment by Sandblasting on the Quality and Electrochemical Corrosion Properties of a C-1020 Carbon Steel Used by an Algerian Oil Company. MATEC Web Conf. **2019**, 272, 01001. https://doi.org/10.1051/matecconf/201927201001.

29 Zhang, H.; Liu, Y.; Yuan, J.; Zhu, M.; Chen, J.; Wang, Z. The Influence of Substrate Surface Treatment on the Electrodeposition of (Co,Mn) 3 O 4 Spinel Precursor Coatings. Mater. Res. Express **2020**, 7 , 076405. https://doi.org/10.1088/2053-1591/aba349.

30 Zhang, Z.; Shen, Z.; Wu, H.; Li, L.; Fu, X. Study on Preparation of Superhydrophobic Ni-Co Coating and Corrosion Resistance by Sandblasting–Electrodeposition. Coatings **2020**, 10, 1164. https://doi.org/10.3390/coatings10121164.

31 Nyambura, S. M.; Kang, M.; Zhu, J.; Liu, Y.; Zhang, Y.; Ndiithi, N. J. Synthesis and Characterization of Ni-W/Cr2O3 Nanocomposite Coatings Using Electrochemical Deposition Technique. Coatings **2019**, 9 . https://doi.org/10.3390/coatings9120815.

32 Zhang, H.; Liu, Y.; Yuan, J.; Zhu, M.; Chen, J.; Wang, Z. The Influence of Substrate Surface Treatment on the Electrodeposition of (Co,Mn)3O4 Spinel Precursor Coatings. Mater. Res. Express **2020**, 7, 076405. https://doi.org/10.1088/2053-1591/aba349.

33 Ding, L.; Torbati-Sarraf, H.; Poursaee, A. The Influence of the Sandblasting as a Surface Mechanical Attrition Treatment on the Electrochemical Behavior of Carbon Steel in Different PH Solutions. Surf. Coatings Technol. **2018**, 352 , 112–119. https://doi.org/10.1016/j.surfcoat.2018.08.013.

34 Liu, Z.; Gao, W. Electroless Nickel Plating on AZ91 Mg Alloy Substrate. Surf. Coatings Technol. **2006**, 200 , 5087–5093. https://doi.org/10.1016/j.surfcoat.2005.05.023.

35 Vitry, V.; Kanta, A.-F.; Delaunois, F. Initiation and Formation of Electroless Nickel–Boron Coatings on Mild Steel: Effect of Substrate Roughness. Mater. Sci. Eng. B **2010**, 175, 266–273. https://doi.org/10.1016/j.mseb.2010.08.003.

36 Nam, D.; Eriksson, F.; Leisner, P.; Zanella, C. Effect of SiC Particle Size and Heat-Treatment on Microhardness and Corrosion Resistance of NiP Electrodeposited Coatings. J. Alloys Compd. **2018**, 769, 1080–1087. https://doi.org/10.1016/j.jallcom.2018.08.013.

37 Jiang, W.; Shen, L.; Xu, M.; Wang, Z.; Tian, Z. Mechanical Properties and Corrosion Resistance of Ni-Co-SiC Composite Coatings by Magnetic Field-Induced Jet Electrodeposition. J. Alloys Compd. **2019**, 791, 847–855. https://doi.org/10.1016/j.jallcom.2019.03.391.

38 Ben Temam, H.; Zeroual, L.; Chala, A.; Rahmane, S.; Nouveau, C. Microhardness and Corrosion Behavior of Ni-SiC Electrodeposited Coatings. Plasma Process. Polym. **2007**, 4 , S618–S621. https://doi.org/10.1002/ppap.200731417.

39 Jin, P.; Sun, C.; Zhang, Z.; Zhou, C.; Williams, T. Fabrication of the Ni-W-SiC Thin Film by Pulse Electrodeposition. Surf. Coatings Technol. **2020**, 392 , 125738. https://doi.org/10.1016/j.surfcoat.2020.125738.

40 Gyawali, G.; Tripathi, K.; Joshi, B.; Lee, S. W. Mechanical and Tribological Properties of Ni-W-TiB2 Composite Coatings. J. Alloys Compd. **2017**, 721, 757–763. https://doi.org/10.1016/j.jallcom.2017.06.044.

41 Xing, S.; Wang, L.; Jiang, C.; Liu, H.; Zhu, W.; Ji, V. Influence of Y2O3 Nanoparticles on Microstructures and Properties of Electrodeposited Ni–W–Y2O3 Nanocrystalline Coatings. Vacuum **2020**, 181 , 109665. https://doi.org/10.1016/j.vacuum.2020.109665.

42 Fan, Y.; He, Y.; Luo, P.; Shi, T.; Chen, X. Pulse Current Electrodeposition and Properties of Ni-W-GO Composite Coatings. J. Electrochem. Soc. **2016**, 163 , D68–D73. https://doi.org/10.1149/2.0171603jes.

43 Kumar, K. A.; Kalaignan, G. P.; Muralidharan, V. S. Direct and Pulse Current Electrodeposition of Ni – W – TiO 2 Nanocomposite Coatings. Ceram. Int. **2013**, 39 , 2827–2834. https://doi.org/10.1016/j.ceramint.2012.09.054.

44 Jiang, W.; Shen, L.; Qiu, M.; Wang, X.; Fan, M.; Tian, Z. Preparation of Ni-SiC Composite Coatings by Magnetic Field-Enhanced Jet Electrodeposition. J. Alloys Compd. **2018**, 762, 115–124. https://doi.org/10.1016/j.jallcom.2018.05.097.

45 Wang, Y.; Zhou, Q.; Li, K.; Zhong, Q.; Bui, Q. B. Preparation of Ni-W-SiO2 Nanocomposite Coating and Evaluation of Its Hardness and Corrosion Resistance. Ceram. Int. **2015**, 41 , 79–84. https://doi.org/10.1016/j.ceramint.2014.08.034.

46 Li, H.; He, Y.; Fan, Y.; Xu, W.; Yang, Q. Pulse Electrodeposition and Corrosion Behavior of Ni–W/MWCNT Nanocomposite Coatings. RSC Adv. **2015**, 5 , 68890–68899. https://doi.org/10.1039/C5RA09462C.

47 Mosavat, S. H.; Bahrololoom, M. E.; Shariat, M. H. Electrodeposition of Nanocrystalline Zn-Ni Alloy from Alkaline Glycinate Bath Containing Saccharin as Additive. *Appl. Surf. Sci.* **2011**, *257*, 8311–8316. https://doi.org/10.1016/j.apsusc.2011.03.017.

48 Rogal, Ł.; Kalita, D.; Tarasek, A.; Bobrowski, P.; Czerwinski, F. Effect of SiC Nano-Particles on Microstructure and Mechanical Properties of the CoCrFeMnNi High Entropy Alloy. J. Alloys Compd. **2017**, 708, 344–352. https://doi.org/10.1016/j.jallcom.2017.02.274.

59 Yang, Y.; Cheng, Y. F. Mechanistic Aspects of Electrodeposition of Ni-Co-SiC Compositenano-Coating on Carbon Steel. Electrochim. Acta. **2013**, 109, 638–644. https://doi.org/10.1016/j.electacta.2013.07.106.

50 Mahmudi, R. Grain Boundary Strengthening in a Fine Grained Aluminium Alloy. Scr. Metall. Mater. **1995**, 32 , 781–786. https://doi.org/10.1016/0956-716X(95)91603-M.